catalysts

MDPI

Article

Optimizing MgO Content for Boosting γ-Al_2O_3-Supported Ni Catalyst in Dry Reforming of Methane

Abdulaziz Bagabas [1,*], Ahmed Sadeq Al-Fatesh [2,*], Samsudeen Olajide Kasim [2], Rasheed Arasheed [1], Ahmed Aidid Ibrahim [2], Rawan Ashamari [1], Khalid Anojaidi [1], Anis Hamza Fakeeha [2], Jehad K. Abu-Dahrieh [3] and Ahmed Elhag Abasaeed [2]

1 National Petrochemical Technology Center (NPTC), Materials Science Research Institute (MSRI), King Abdulaziz City for Science and Technology (KACST), Riyadh 11442, Saudi Arabia; rrisheed@kacst.edu.sa (R.A.); ralshammary@kacst.edu.sa (R.A.); khalid.alnjaidi@gmail.com (K.A.)

2 Chemical Engineering Department, College of Engineering, King Saud University, Riyadh 11421, Saudi Arabia; sofkolajide2@gmail.com (S.O.K.); aidid@ksu.edu.sa (A.A.I.); anishf@ksu.edu.sa (A.H.F.); abaseedi@ksu.edu.sa (A.E.A.)

3 School of Chemistry and Chemical Engineering, Queen's University Belfast, Belfast BT9 5AG, UK; j.abudahrieh@qub.ac.uk

* Correspondence: abagabas@hotmail.com (A.B.); aalfatesh@ksu.edu.sa (A.S.A.-F.); Tel.: +966-56-983-1338 (A.B.); +966-11-467-6859 (A.S.A.-F.)

Abstract: The dry reforming of methane (DRM) process has attracted research interest because of its ability to mitigate the detrimental impacts of greenhouse gases such as methane (CH_4) and carbon dioxide (CO_2) and produce alcohols and clean fuel. In view of this importance of DRM, we disclosed the efficiency of a new nickel-based catalyst, which was promoted with magnesia (MgO) and supported over gamma-alumina (γ-Al_2O_3) doped with silica (SiO_2), toward DRM. The synthesized catalysts were characterized by H_2 temperature-programmed reduction (H_2-TPR), X-ray diffraction (XRD), X-ray Photoelectron Spectroscopy (XPS), Thermogravimetric analysis (TGA), and Transmission electron microscopy (TEM) techniques. The effect of MgO weight percent loading (0.0, 1.0, 2.0, and 3.0 wt. %) was examined because the catalytic performance was found to be a function of this parameter. An optimum loading of 2.0 wt. % of MgO was obtained, where the conversion of CH_4 and CO_2 at 800 °C were 86% and 91%, respectively, while the syngas (H_2/CO) ratios relied on temperature and were in the range of 0.85 to 0.95. The TGA measurement of the best catalyst, which was operated over a 15-h reaction time, displayed negligible weight loss (<9.0 wt. %) due to carbon deposition, indicating the good resistance of our catalyst system to the deposition of carbon owing to the dopant and the modifier. TEM images showed the presence of multiwalled carbon nanotubes, confirming the TGA.

Keywords: methane; carbon dioxide reforming; magnesium oxide; γ-alumina doped with silica

check for updates

Citation: Bagabas, A.; Al-Fatesh, A.S.; Kasim, S.O.; Arasheed, R.; Ibrahim, A.A.; Ashamari, R.; Anojaidi, K.; Fakeeha, A.H.; Abu-Dahrieh, J.K.; Abasaeed, A.E. Optimizing MgO Content for Boosting γ-Al_2O_3-Supported Ni Catalyst in Dry Reforming of Methane. *Catalysts* **2021**, *11*, 1233. https://doi.org/10.3390/catal11101233

Academic Editor: Hamidreza Arandiyan

Received: 9 September 2021
Accepted: 9 October 2021
Published: 13 October 2021

1. Introduction

Synthesis gas (syngas), a mixture of hydrogen (H_2) and carbon monoxide (CO), is a vital material for the synthesis of useful liquid fuels, such as methyl alcohol and dimethyl ether, through a Fischer–Tropsch process [1,2]. The widely used procedures for the syngas manufacturing are methane steam reforming, dry reforming, and partial oxidation [3]. The DRM, shown in Equation (1), has gained great attention because the H_2/CO mole ratio is near one, and this ratio is suitable for utilization in the Fischer–Tropsch process, in fuel cells, and in the production of chemicals [4].

$$CH_4 + CO_2 = 2CO + 2H_2 \qquad \Delta H^0_{298} = 260.5\frac{kJ}{mol} \tag{1}$$

In addition, DRM transforms the main two greenhouse gases, CH_4 and CO_2, into syngas [5].

Moreover, DRM is an attractive means for utilizing natural gas and biogas composed of CH_4 and CO_2 as the main constituents [6].

The catalysts used for DRM could be deactivated because of coke deposition from CH_4 decay and Boudouard reaction, as denoted in Equations (2) and (3), respectively. In addition, rapid deactivation can be caused by sintering and metallic oxidation of catalyst, as a result of the endothermic nature of DRM (Equation (1)), which requires high temperature to achieve high conversion of the reactants [7]. Nevertheless, the primary factor for catalyst deactivation has been considered to be coke deposition [8].

$$CH_4 = C + 2H_2 \qquad \Delta H^0_{298} = 75.0 \frac{kJ}{mol} \tag{2}$$

$$2CO = C + CO_2 \qquad \Delta H^0_{298} = -172.0 \frac{kJ}{mol} \tag{3}$$

Catalysts based on noble metals (such as rhodium, ruthenium, platinum, and palladium) and non-noble metals such as nickel (Ni) and cobalt (Co) have been widely studied in DRM. [5] On one hand, high catalytic performance and high resistance to coke formation were perceived in the noble metal-based catalysts. However, their use has been limited due to their expensiveness and rarity. On the other hand, low cost and comparable activity have made Ni-based catalysts good substitutes, but coke deposition and sintering are two important difficulties for emerging Ni-based catalysts at the industrial level. The influences of the method of synthesis, variation of support, promoters, operating circumstances, and reactor configurations can be altered to enhance the performance and steadiness of the Ni-based catalysts [8].

A conventional approach for improving the activity and steadiness of Ni-based catalysts is to employ appropriate promoters of metals and/or their oxides. In this regard, cerium oxide promoter has been extensively used due to its high capacity for storing oxygen and for cerium high redox properties, Ce^{4+}/Ce^{3+} [9–11]. Thus, higher activity and higher coke deposition resistance have been obtained for Ni-based catalysts promoted with Ce-containing material [12]. Sepehri et al. [5,9] reported the high activity and high coke resistance of Al_2O_3-supported Ni catalyst promoted with 3.0 wt. % of Ce in methane partial oxidation reactions. Furthermore, Kim et al. [13] reported better activities for CeO_2-promoted Ni/γ-Al_2O_3 catalyst than the unpromoted one. The promoted catalyst exhibited higher activity because of the interaction between Ni and Ce, forming the new active sites for converting methane. In addition, Mattos et al. [14] reported better activity and steadiness for Pt/Ce-ZrO_2 in comparison to Pt/ZrO_2. The good performance of Pt/Ce-ZrO_2 was owed to the enhancement of coke gasification by the CeO_2 higher oxygen mobility. Taherian et al. proved that Ni/SBA-16-Mg, promoted with 3% either Ce or Y, resulted in highly dispersed nickel nanoparticles, having an average size of 11.5 nm, and in oxygen vacancies in the support. Their catalyst combination had a remarkable enhancement of catalytic activity and stability [15]. Al-Fatesh et al. promoted nickel catalyst over mesoporous zirconia for DRM by using various loadings of MgO. They found that the potent interaction of NiO–MgO solid solution with the ZrO_2 support was essential for obtaining high conversions of both methane and carbon dioxide. Furthermore, over their mixture of metal oxides, carbon dioxide functioned as a soft oxidizing for surface coke, entailing the stability of catalytic performance [16]. Karam et al. found the optimum loading of MgO was in the range of 5–10 wt. % for the mesoporous Ni_6-Mg_x-Al_2O_3, prepared by one-pot evaporation-induced self-assembly, for DRM due to lower activation energy [17]. In another study conducted by Bahare et al. [18], MgO-promoted Ni/$MgSiO_3$ showed the highest catalytic performance among the unpromoted and those promoted with other metal oxides. They concluded that the addition of MgO increased Ni dispersion and provided suitable Ni active sites for the reactants. Alipour et al. [19] also reported an enhancement of methane conversion in DRM when MgO was added to Ni/Al_2O_3 catalyst. The advantage of incorporating MgO in the catalyst matrix was revealed by the work of Shen et al. [20], where oxidative DRM was performed for 100 h on stream over Ni supported on $MgAl_2O_4$

spinel. The result displayed a stable performance of high CH_4 conversion with no deactivation owing to sintering or coke deposition. Cho et al. investigated the impact of Mg/Al mole ratio of $MgAl_2O_4$ mesoporous support on the catalytic activity of nickel in DRM. They found the best coke resistance, proper acidity, and defect structure when the Mg/Al mole ratio was 0.24 [21]. Hu and Ruckenstein [22] highlighted the benefits of the solid solution of NiO-MgO for DRM. The basic property of MgO and its similar lattice parameters to that of NiO resulted in a catalyst of NiO-MgO solid solution, which showed the highest conversions for carbon dioxide and methane with resistance to carbon deposition. Silica (SiO_2) is also considered as a promising support modifier due to its great physicochemical properties. Silica has been reported to facilitate the reduction of NiO species by weakening its interaction with the metal oxide support [23]. However, the weak metal support interaction could lead to quick deactivation as a result of agglomeration of active metal species. Several investigators applied modified silica support in upgrading the catalytic activity, stability, and in overcoming the deactivation problems by adding elements such as lithium, lanthanum, cerium, magnesium, cobalt, niobium, and zinc [24–27]. On the other hand, Al_2O_3 interacts strongly with NiO, facilitating the development of the spinel phase of $NiAl_2O_4$ and therefore complicating the reduction to nickel metal [23]. Yadav et al. showed that the catalytic activity of perovskite-type catalyst of $40LaNi_{0.75}Zr_{0.25-x}CexO_3/SiO_2$, modified with alumina or magnesia, was improved due to the formation of nickel aluminate or solid solution of nickel-magnesia, which increased the basicity of silica and hence improved both the reactant conversions and product yield in DRM [28]. The importance of an MgO promoter and SiO2 support modifier for Ni-based catalysts toward the activity and stability performance in DRM stipulates the optimization of MgO loading for well-defined modified support of alumina.

In this research work, the catalytic performance of 5.0 wt. % NiO catalyst, promoted with MgO and supported on gamma-alumina doped with 3.0 wt. % SiO_2, was investigated for DRM. The effect of MgO wt. % loading (0.0, 1.0, 2.0, and 3.0) was investigated on the catalyst activity and stability, which is expressed in conversions of methane and carbon dioxide, and the molar ratio of H_2/CO.

2. Results and Discussion

To observe the reproducibility and the consistence of the obtained data, blank tests and carbon balances were performed. The mass balance, in respect to carbon and overall, was within ±5% for all catalysts. The experiment was repeated three times for each run, resulting in consistent values with a percentage error within 3%. To comprehend differences in the performance of the prepared catalysts, nitrogen adsorption–desorption isotherms of the catalysts were registered for investigating the textural attributes: specific surface area (S_{BET}), pore volume (P_v), and pore diameter (P_d). Figure 1 displays the nitrogen adsorption–desorption isotherms (Figure 1), which indicated the mesoporous nature of the prepared catalysts because the isotherms were of type IV with a hysteresis loop of the H1-type, owing to the condensation in and evaporation from capillaries at relatively high pressures. This structural characteristic is known for hexagonal array and mesoporous SiO_2-Al_2O_3 [29]. The loading of both the active metal and promoter did not noticeably change the framework of the support. However, a significant increase in the relative pressure region of 0.65–0.95 was observed owing to a combination of N_2 capillary condensation within the mesopores and the interstitial cavities of the SiO_2-AlO_3. The physisorption results are as shown in Table 1, which shows that the 5Ni2Mg3SiAl has the highest surface area of all catalysts, implying that most of the active catalyst and promoter particles are exposed to the reactants. Thus, the chance of colliding reactants with the catalyst surface is high, leading to more successful collisions per second, a higher reaction rate, and better activity performance.

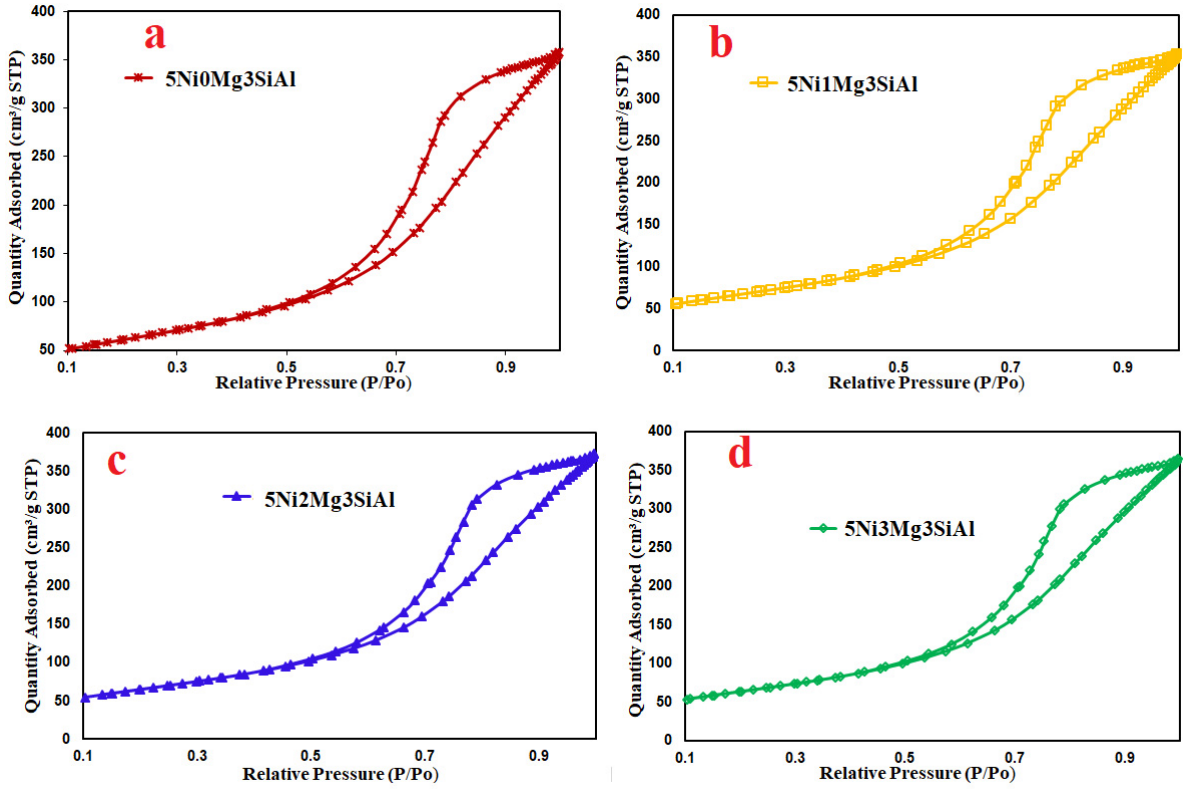

Figure 1. N_2 adsorption–desorption isotherms of the fresh 5Ni0Mg3SiAl (**a**), 5Ni1Mg3SiAl (**b**), 5Ni2Mg3SiAl (**c**), and 5Ni3Mg3SiAl (**d**) catalysts.

Table 1. The results of nitrogen physisorption for the various catalysts.

Catalyst	S_{BET} (m^2/g)	P_v (cm^3/g)	P_d (nm)
3SiAl	262.59	0.69	9.69
5Ni0Mg3SiAl	222.08	0.59	9.21
5Ni1Mg3SiAl	235.17	0.57	9.08
5Ni2Mg3SiAl	236.60	0.61	9.13
5Ni3Mg3SiAl	230.15	0.60	9.13

The Barrett–Joyner–Halenda (BJH) pore size distribution is shown in Figure 2.

A monomodal pore size distribution was observed for all the prepared catalysts, where the peak was located in the micropore and mesopore range (0–500 Å), confirming the results of N_2 adsorption–desorption isotherms. In addition, a small tail in the macropore range (>500 Å) was observed for every prepared catalyst, but such pores would have a negligible effect on the textural properties.

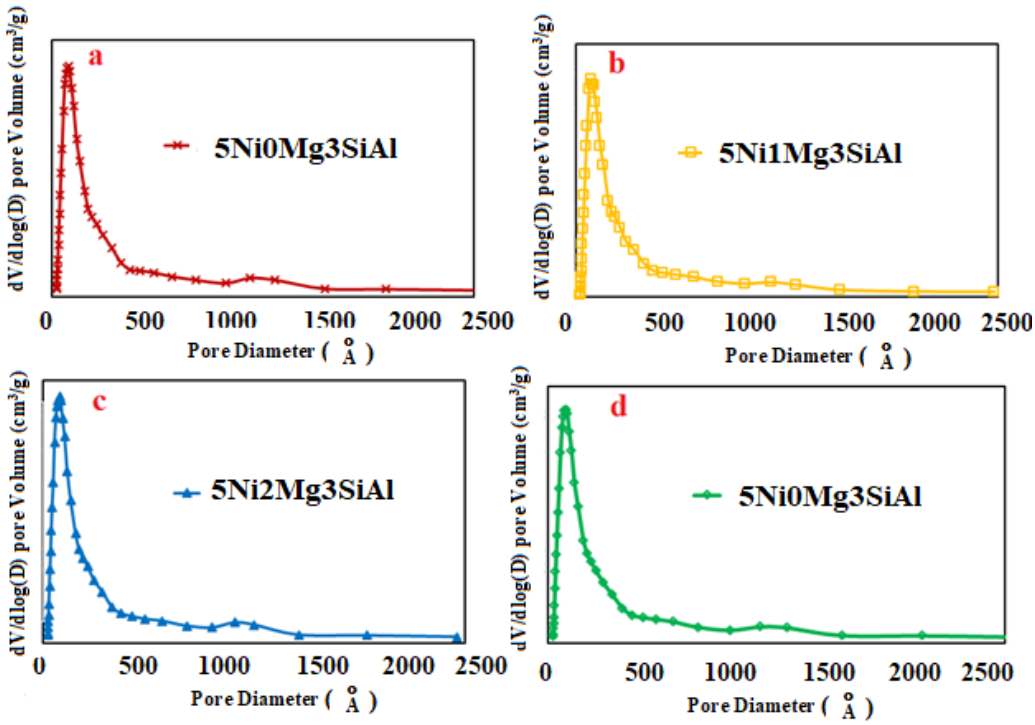

Figure 2. BJH pore size distributions for the fresh 5Ni0Mg3SiAl (**a**), 5Ni1Mg3SiAl (**b**), 5Ni2Mg3SiAl (**c**), and 5Ni3Mg3SiAl (**d**) catalysts.

2.1. H_2-TPR

To investigate the reducibility of the prepared catalysts, the hydrogen temperature-programmed reduction (H_2-TPR) is a helpful tool. The H_2-TPR profiles are illustrated in Figure 3. All the prepared catalysts exhibited a negative intensity zone besides three reduction zones: low (I), moderate (II), and high (III) temperatures, where the metal oxide species were reduced as per their degree of interaction with and their dispersion on the support. The negative intensity zone could be ascribed to the spillover of hydrogen in the mesopores of the support [30]. The peaks, observed in the low-temperature (I) zone of 200–400 °C, could be ascribed to the dispersion of slight quantities of free NiO nanoparticles, which interacted weakly with the support [31]. All the prepared catalysts displayed a broad reduction peak in the moderate zone, centered around 400–700 °C, which might be due to the modest interaction between the support and the NiO. The 5Ni1Mg3SiAl catalyst exhibited another small peak centered around 450 °C. The catalysts showed strong interaction between support and the NiO due to the reduction of Ni^{2+} in the extremely crystalline NiO [22]. The 5Ni2Mg3SiAl catalyst displayed the best catalytic performance owing to the best NiO interaction with the support in the moderate-temperature (II) region, while the 5Ni3Mg3SiAl catalyst showed inferior catalytic performance because it had a stronger NiO interaction with the support, hindering the reduction of NiO. The 5Ni1Mg3SiAl catalyst showed a little bit lower performance than the 5Ni3Mg3SiAl catalyst because the free NiO particles would facilitate the sintering of Ni particles with the progress of DRM reaction. Table 2 displays the H_2-consumption during TPR; the H_2-consumption values during the TPR study indicated that negligible absorption took place at both lower and higher temperature zones. The considerable absorption happened at the moderate temperature zone between 650 and 705 °C. The best catalyst 5Ni2Mg3SiA with the appropriate NiO interaction with the support gave the lowest H_2- consumption value.

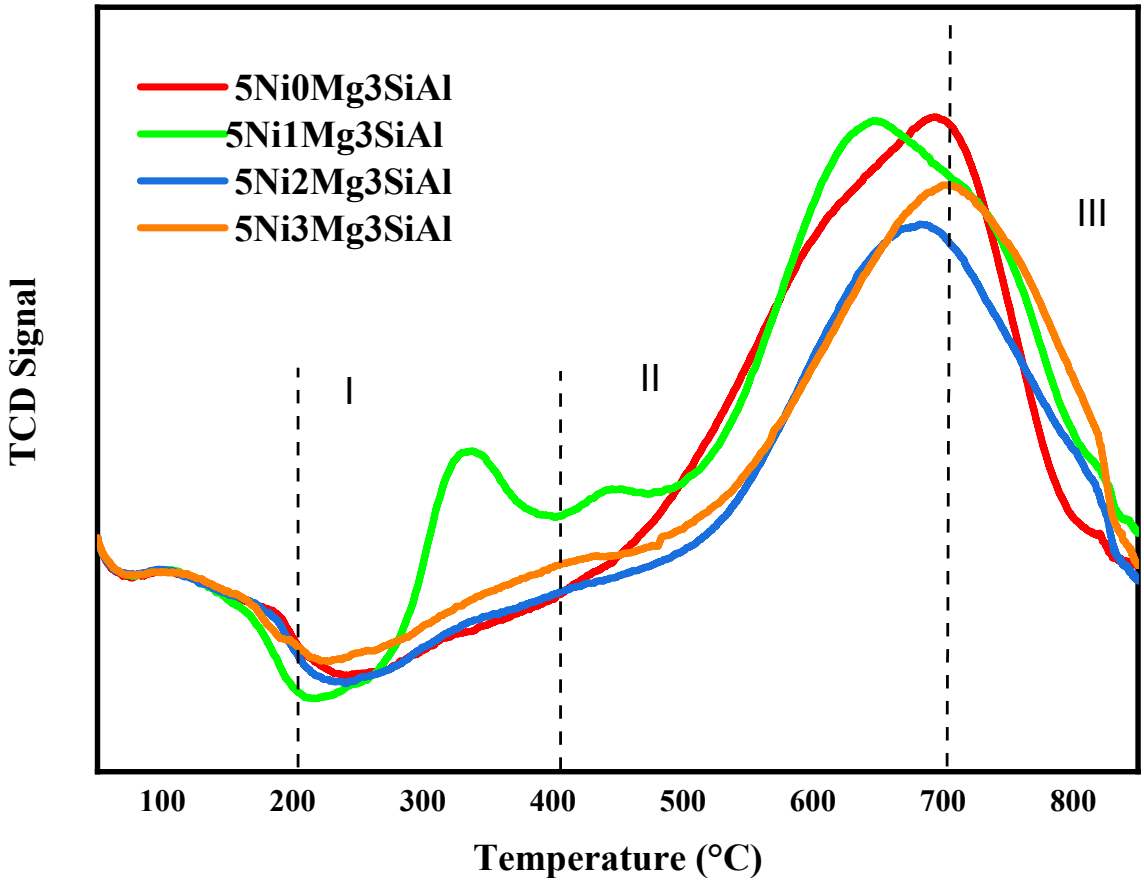

Figure 3. The H_2-TPR profiles of the fresh 5Ni0Mg3SiAl, 5Ni1Mg3SiAl, 5Ni2Mg3SiAl, and 5Ni3Mg3SiAl catalysts.

Table 2. H_2-consumption during TPR.

Catalyst	Temperature (°C)	H_2-Consumption (μmole/g)
5Ni0Mg3SiAl	697.9	951.1
	833.0	1.0
	841.4	0.9
5Ni1Mg3SiAl	336.6	53.2
	438.5	0.7
	454.8	30.1
	649.9	992.0
	850.2	5.8
5Ni2Mg3SiA	687.1	789.4
	846.3	0.5
	846.5	2.1
	851.1	1.1
	854.1	0.7
5Ni3Mg3SiAl	705.1	887.7
	844.4	13.5
	852.9	1.4
	855.6	1.1

2.2. X-ray Diffraction (XRD)

Figure 4 shows the XRD patterns of the prepared catalysts. The diffraction peaks at 2θ = 37.2°, 45.5°, and 67° were ascribed to γ-Al_2O_3 (JCPDS file No.: 29-0063).

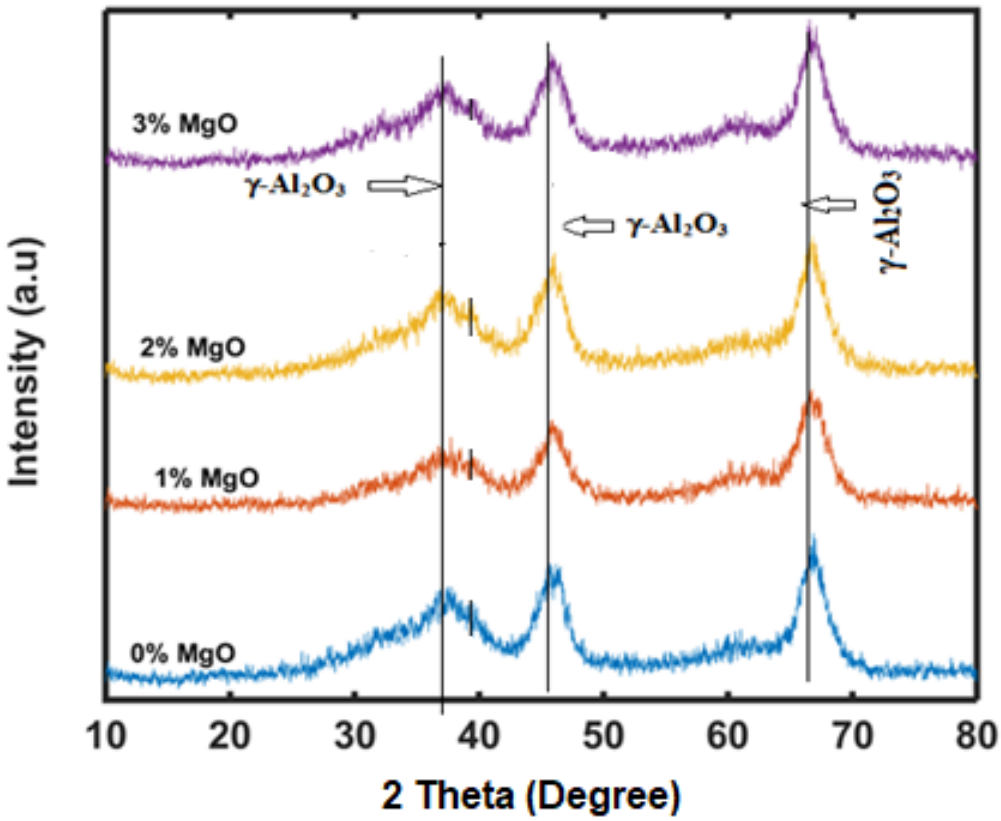

Figure 4. The XRD patterns of the fresh 5Ni0Mg3SiAl, 5Ni1Mg3SiAl, 5Ni2Mg3SiAl, and 5Ni3Mg3SiAl catalysts.

2.3. XPS

The O1s XPS (Figure 5a) had a peak centered at 532.3 eV for 5Ni0Mg3SiA, at 532.7 eV for 5Ni1Mg3SiAl and 5Ni2Mg3SiAl, and at 532.4 eV for 5Ni3Mg3SiAl. The presence of Si and absence of Mg in 5Ni0Mg3SiA shifted the O1s binding energy to higher energy than that of γ-Al_2O_3 (531.08 eV) [30], which could be ascribed to the incorporation of Si into the lattice of γ-Al_2O_3. The incorporation of Mg led to an increase in the O1s binding energy, which might be due to peroxide species (O_2^{2-}) or to hydroxyl species and most probably due to hydroxyl species. [32] The reduction in O1s binding energy upon increasing the MgO to 3.0 wt. % could be attributed to the higher interaction between MgO and NiO, which, in turn, led to a solid solution between them, and hence, an increased difficulty of reducing NiO [32].

The $Ni2p_{3/2}$ peak (Figure 5b) for 5Ni0Mg3SiAl catalyst was observed at 855.02 eV. Upon incorporation of Mg, the $Ni2p_{3/2}$ peak was shifted to 855.39, 855.13, and 854.31 eV for 5Ni1Mg3SiAl, 5Ni2Mg3SiAl, and 5Ni3Mg3SiAl, respectively. All values for $Ni2p_{3/2}$ were less than that of NiO (856.20 eV). This reduction in binding energy could be due to the presence of Ni octahedral lattice sites having electrostatic potential among six negatively-charged oxide with a better opportunity of extra-atomic relaxation [33]. Furthermore, increasing the amount of MgO wt. % loading resulted in more decrease in the binding energy of $Ni2p_{3/2}$. This observation could be attributed to the increase in interaction between MgO and NiO with increasing the loading wt. % of MgO [32]. The additional peak at ≈864 eV could be due to the solid solution of MgO-NiO.

The Al2p peaks (Figure 5c) of 5Ni0Mg3SiAl, 5Ni1Mg3SiAl, 5Ni2Mg3SiAl, and 5Ni3Mg3SiAl catalysts were observed at 74.03, 74.96, 75.53, and 74.56 eV, respectively. The value of Al2p binding energy of 5Ni0Mg3SiAl was very close to that of γ-Al_2O_3 (74.30 eV). This red shift in binding energy could be owing to the presence of Si in the lattice of γ-Al_2O_3. However, the incorporation of MgO led to an increase in the binding energy of Al2p, which could

be due to the interaction of MgO with γ-Al_2O_3 support. This interaction between MgO and the support reached its maximum when the MgO loading was 2.0 wt. %. The XPS results were in agreement with the observed catalytic performance, which showed that 5Ni2Mg3SiAl was the best catalyst.

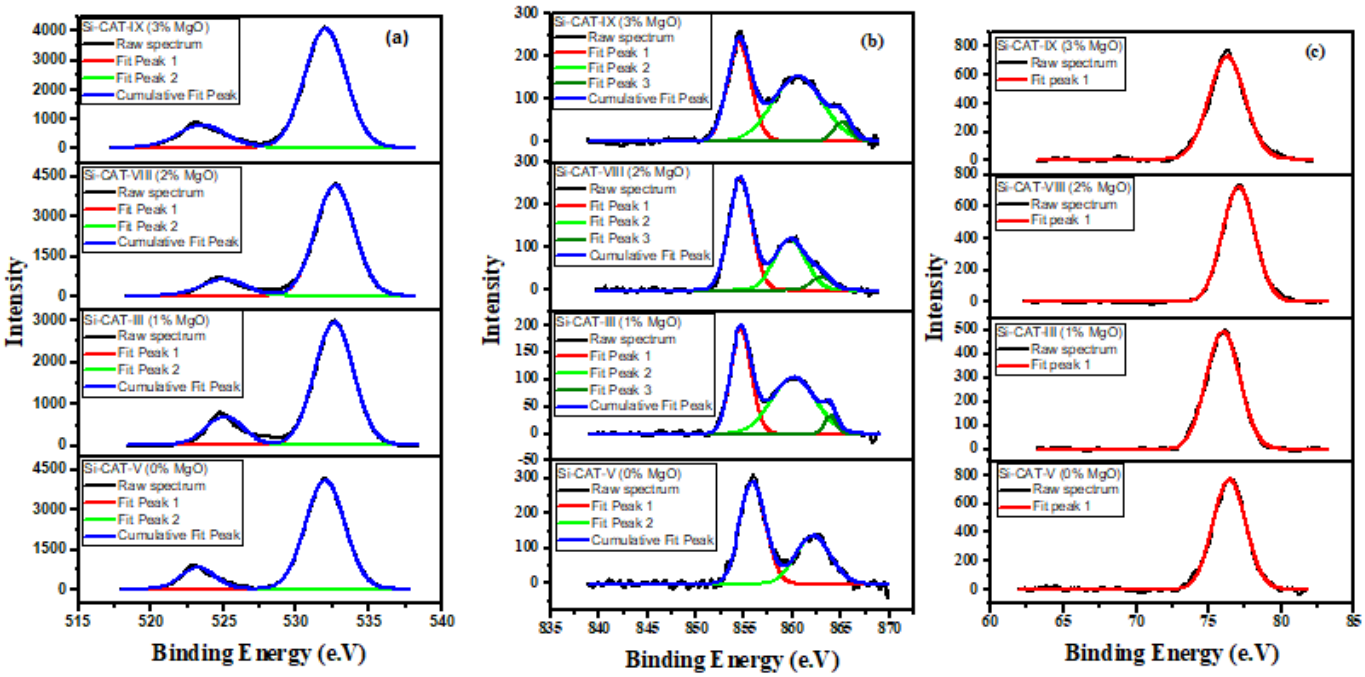

Figure 5. (**a**) O1s, (**b**) Ni2p, and (**c**) Al2p XP spectra of the fresh 5Ni0Mg3SiAl, 5Ni1Mg3SiAl, 5Ni2Mg3SiAl, and 5Ni3Mg3SiAl catalysts.

2.4. The Catalytic Activity and Stability

The catalytic performances of the catalysts in the DRM process were evaluated at 700 °C for 420 min. Figure 6a shows that the CH_4 conversion improved slightly by incorporating 1.0 wt. % and 3.0 wt. % loadings of MgO in comparison to the catalyst without MgO. This increase in CH_4 conversion might be due to the supplementary metal active sites endowed by MgO. On the other hand, 2.0 wt. % loading of MgO raised the CH_4 conversion markedly by about 16% in comparison with the catalyst without MgO. These results showed the preferential effect of loading MgO on the conversion of CH_4. Similarly, Figure 6b displays the effect of different MgO wt. % loadings on CO_2 conversion. The CO_2 conversion was enhanced with the promotion of MgO, where the 2.0 wt. % loading of MgO improved the conversion by ≈8%. In addition, the higher CO_2 conversion hinted at the incidence of a reverse water gas shift (RWGS) process (Equation (4)).

$$CO_2 + H_2 \rightarrow CO + H_2O \quad (4)$$

The catalyst with 2.0 wt. % loading of MgO had the best conversions for methane and carbon dioxide, which was followed by the one with 3.0 wt. % loading of MgO. Figure 6c shows the H_2/CO mole ratio profile for different wt. % loading of MgO in the catalyst. The loadings of 1.0 wt. % (5Ni1Mg3SiAl) and 2.0 wt. % (5Ni2Mg3SiAl) were affected by the H_2 consumption of the RWGS reaction (Equation (4)) [34], which led to an increase in the conversion of CO_2 and to a decline in the H_2/CO mole ratio. Similarly, the 5Ni3Mg3SiAl catalyst attained a comparable molar ratio of H_2/CO to the 5Ni2Mg3SiAl catalyst. For the conversions of methane and carbon dioxide and the molar ratio of H_2/CO, the stability was sustained during the 420 min of time-on-stream.

Figure 7 exhibits the impact of reaction temperature on the conversions for methane and carbon dioxide, and the molar ratio of H_2/CO. The methane and carbon dioxide con-

versions, as expected, improved with the increase in temperature because of the endoergic character of DRM. The 5Ni2Mg3SiAl catalyst exhibited relative superiority in the conversion of methane and carbon dioxide. In addition, the molar ratio of H_2/CO increased and a unity value was obtained at 750 °C, while those of other temperatures provided were either lower or higher than one, depending on the involvement of the RWGS reaction (Equation (4)) and Boudouard reaction (Equation (3)).

Figure 8 displays the stability results of the 5Ni2Mg3SiAl catalyst by studying the methane and carbon dioxide conversions and the molar ratio of H_2/CO versus time-on-stream (TOS) for 15 h. The catalyst demonstrated excellent stability and negligible deactivation for both reaction temperatures: 700 °C and 800 °C. The methane and carbon dioxide conversions, by raising the temperature from 700 °C to 800 °C, were improved by 25% and 17%, respectively. The molar ratio of H_2/CO had values less than unity for 700 °C reaction temperature and values above unity for 800 °C. On this basis, reforming at 750 °C would be the optimum reaction temperature for securing the unity ratio, as depicted in Figure 7c.

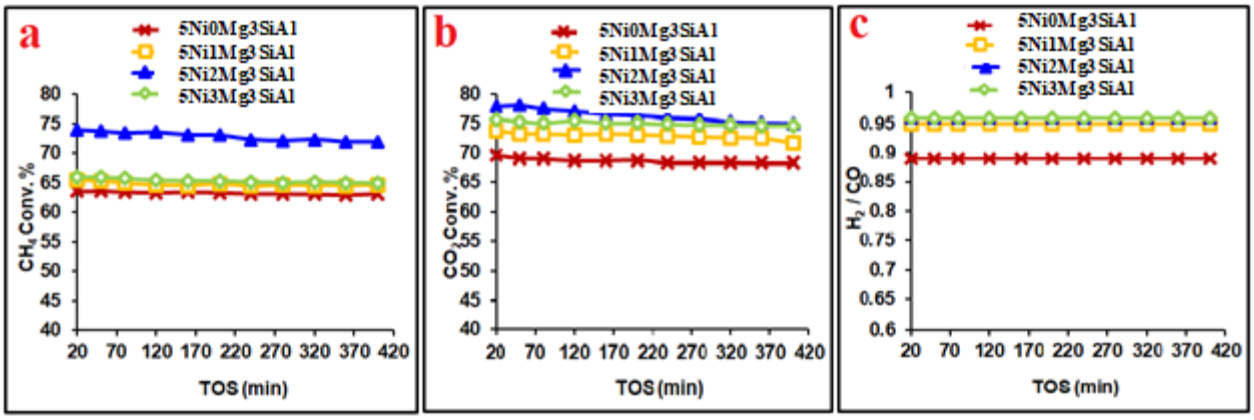

Figure 6. (**a**) CH_4 conversion, (**b**) CO_2 conversion, and (**c**) H_2/CO mole ratio as a function of TOS for the 5Ni0Mg3SiAl, 5Ni1Mg3SiAl, 5Ni2Mg3SiAl, and 5Ni3Mg3SiAl catalysts. Reaction conditions: $CH_4/CO_2/N_2$ = 6/6/1 ($v/v/v$); GHSV = 39,000 mL/g_{cat}/h; M_{cat} = 100 mg; t = 700 °C.

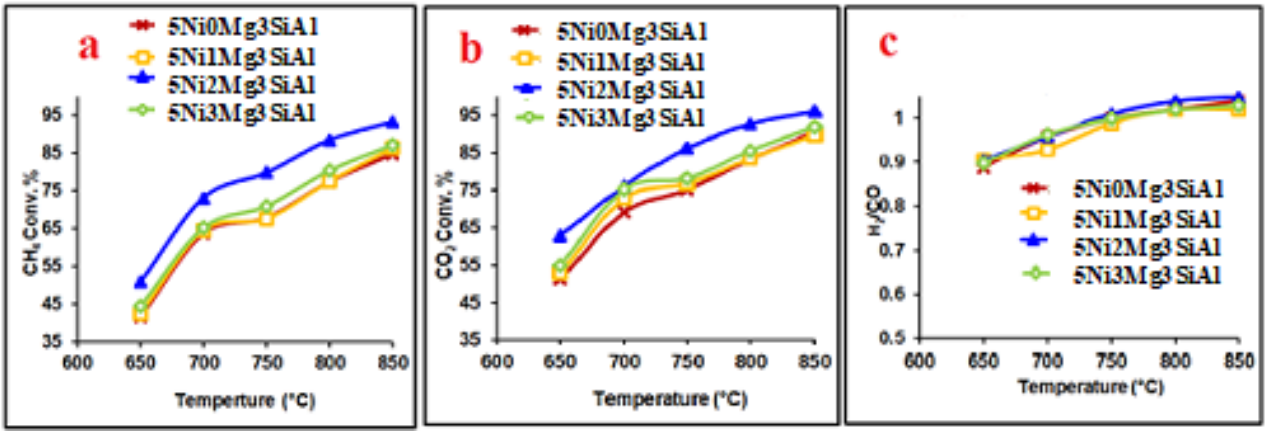

Figure 7. (**a**) CH_4 conversion, (**b**) CO_2 conversion, and (**c**) H_2/CO mole ratio as a function of reaction temperature for the 5Ni0Mg3SiAl, 5Ni1Mg3SiAl, 5Ni2Mg3SiAl, and 5Ni3Mg3SiAl catalysts. Reaction conditions: $CH_4/CO_2/N_2$ = 6/6/1 ($v/v/v$); GHSV = 39,000 mL/g_{cat}/h; M_{cat} = 100 mg.

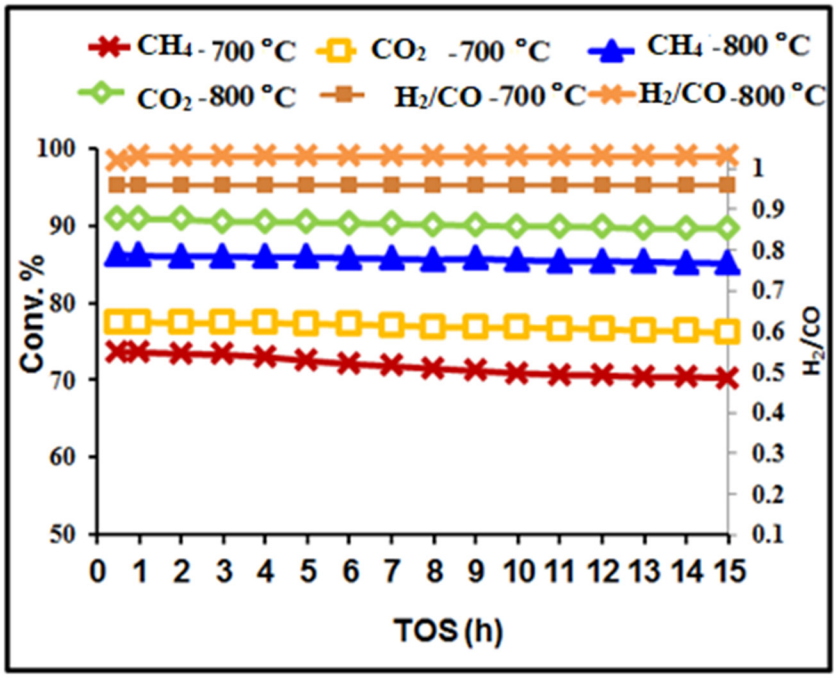

Figure 8. Stability tests of the 5Ni2Mg3SiAl catalyst in terms of conversions of CH_4 and CO_2 and H_2/CO mole ratios. Reaction conditions: t = 700 or 800 °C; GHSV = 39,000 mL/g_{cat}/h; P = 1.0 atm.

2.5. Space Velocity

The impact of contact time on the conversion of methane and carbon dioxide over 5Ni0Mg3SiAl, 5Ni1Mg3SiAl, 5Ni2Mg3SiAl, and 5Ni3Mg3SiAl catalysts was investigated at 700 °C and with a molar ratio of unity for methane to carbon dioxide by varying the gas hourly space velocity (GHSV). Figure 9 displays the results for 5Ni2Mg3SiAl catalyst. The CH_4 conversion profile displayed two aspects. When the GHSV was increased from 39,000 mL/g_{cat}/h to 78,000 mL/g_{cat}/h, the CH_4 conversion was reduced from about 73% to 55%. This observation was expected because when the contact time was decreased by increasing the GHSV, the reactants could not adequately interact with the active Ni and Mg particles. Therefore, some of the reactants were left unreacted. Furthermore, high GHSV was not favorable for CH_4 conversion because of the use of short bed length [34]. On the other hand, when GHSV was reduced to 19,500 mL/g_{cat}/h, the CH_4 conversion also decreased. This observation could be ascribed to the mass transfer limitations. The impact of GHSV on the molar ratio of H_2/CO (Figure 9) indicated that this ratio reduced as GHSV increased from 19,500 mL/g_{cat}/h. This observation could be attributed to the mass transfer limitations and to the RWGS reaction (Equation (4)), which caused additional CO_2 conversion and a decrease in the molar ratio of H_2/CO [35]. The relative increase in the molar ratio of H_2/CO from 39,000 to 78,000 mL/g_{cat}/h could be due to the decomposition of methane and the occurrence of WGS reaction of CO with H_2 to produce CH_4.

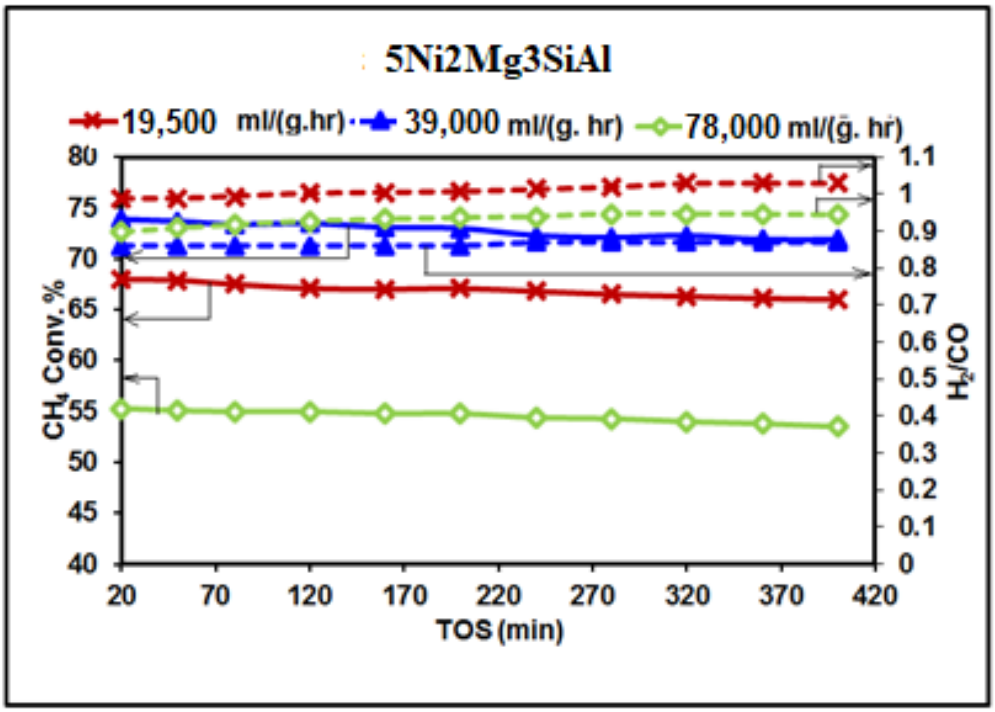

Figure 9. The impact of GHSV on CH_4 conversion and H_2/CO mole ratio (Reaction conditions: CH_4: CO_2 mole ratio = 1; catalyst: 5Ni2Mg3SiAl; t = 700 °C; P = 1 atm).

2.6. Thermogravimetric Analysis (TGA)

The TGA measurements in Figure 10 gave a weight loss in the range of 5–9 wt. % and indicated that the amount of carbon deposition was comparable over the tested catalysts within a reaction time of 420 min at 700 °C. The addition of MgO and its loading increase marginally improved the stability. Nonetheless, TGA measurement for a longer period of 15 h (Figure 11) showed that the catalyst with 2.0 wt. % MgO maintained the same range of weight loss (<9.0 wt. %), displaying that the catalyst had a good resistance toward coke formation and possessed excellent stability.

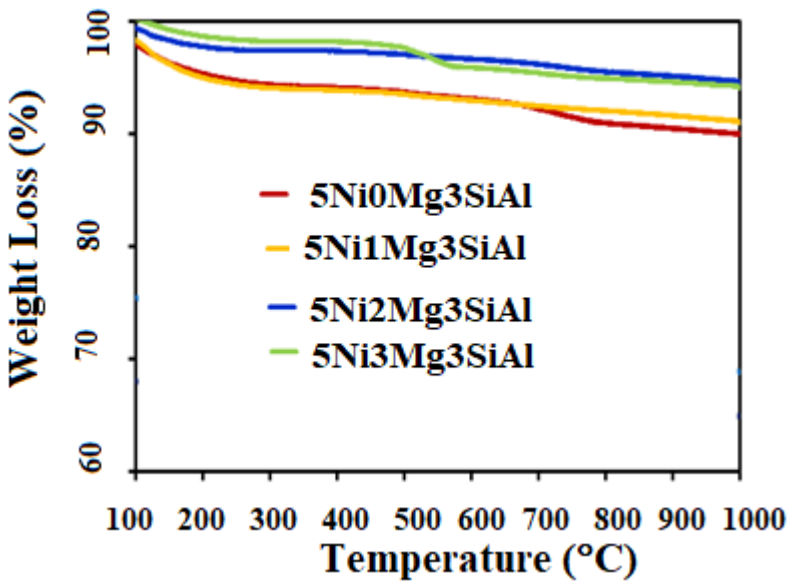

Figure 10. The weight loss curves measured over the spent 5Ni0Mg3SiAl, 5Ni1Mg3SiAl, 5Ni2Mg3SiAl, and 5Ni3Mg3SiAl catalysts tested for 420 min.

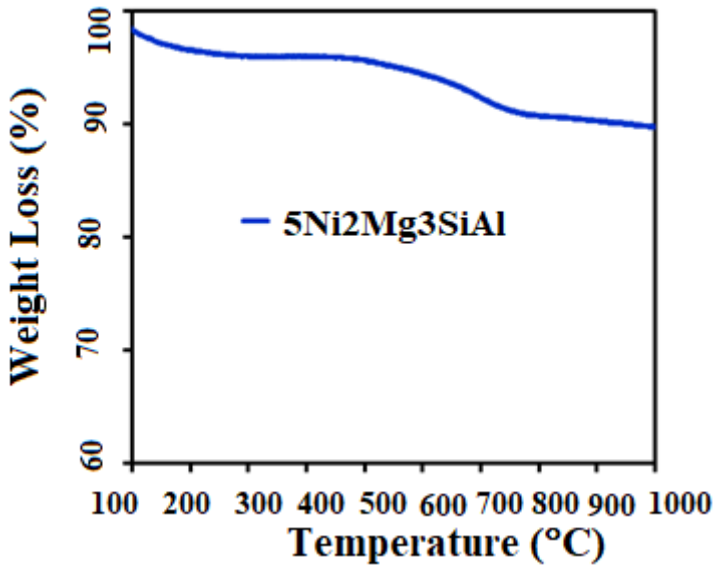

Figure 11. The weight loss curve measured over the spent 5Ni2Mg3SiAl catalyst tested for 15 h.

2.7. Transmission Electron Microscopy (TEM) Analysis

We found that our prepared catalysts were made of agglomerated nanorods, as shown in Figure 12 for the 5Ni2Mg3SiAl catalyst. The length of these nanorods was in the range of 20–50 nm (Figure 12a), while their diameter fell in the range of 2–5 nm (Figure 12b). This observed morphological nature could be responsible for the low intensity of the XRD patterns and the good resistance of the catalysts toward the deposition of carbon.

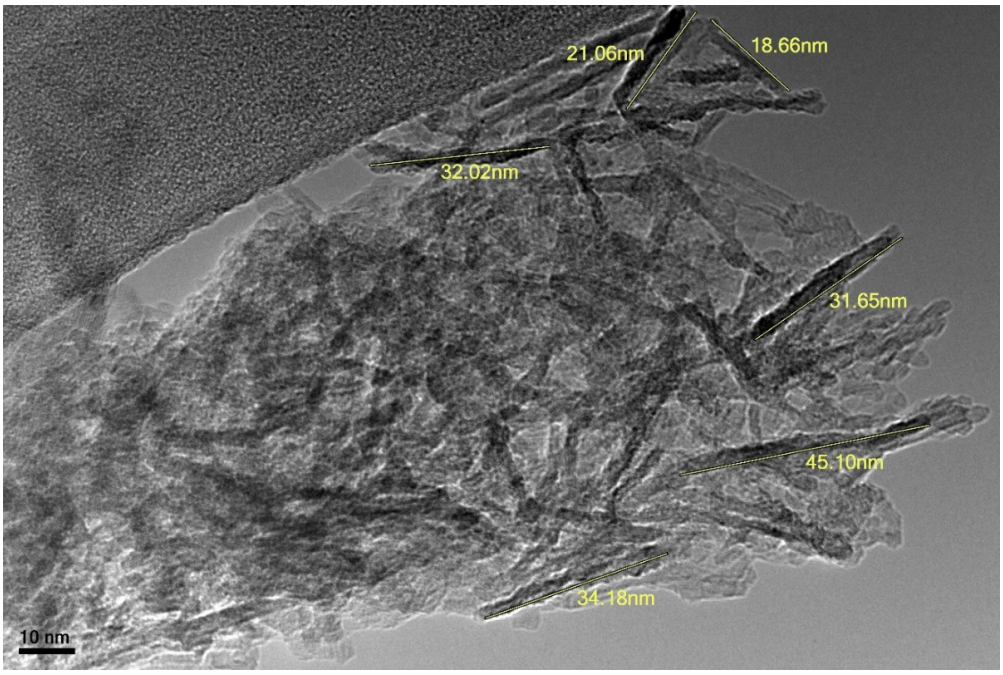

(**a**)

Figure 12. *Cont.*

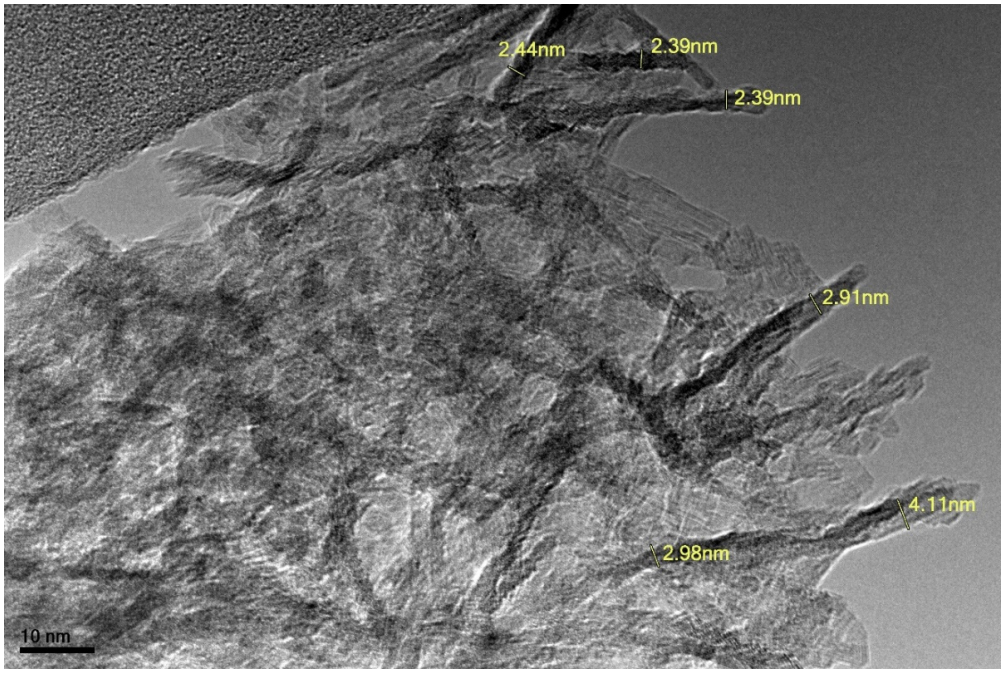

(**b**)

Figure 12. TEM images for the fresh sample of 5Ni2Mg3SiAl, showing the length of some nanorods (**a**) and the diameter of some others (**b**).

Figure 13 shows the TEM images of the spent sample of 5Ni2Mg3SiAl. Figure 13a clearly shows the formation of multiwalled carbon nanotube (MWCNT), surrounded by the agglomerated catalyst particles, which had their shapes changed from rod-like to undefined. The outer diameter of the MWCNT was larger than its internal diameter. Both diameters were not the same along the MWCNT, as shown in Figure 13a. The distance between one wall and another was estimated to be ≈0.35 nm, as shown in Figure 13b. The formation of MWCNT and change in the morphology of the catalyst particles would be responsible for reduction of the catalyst activity along with the reaction time.

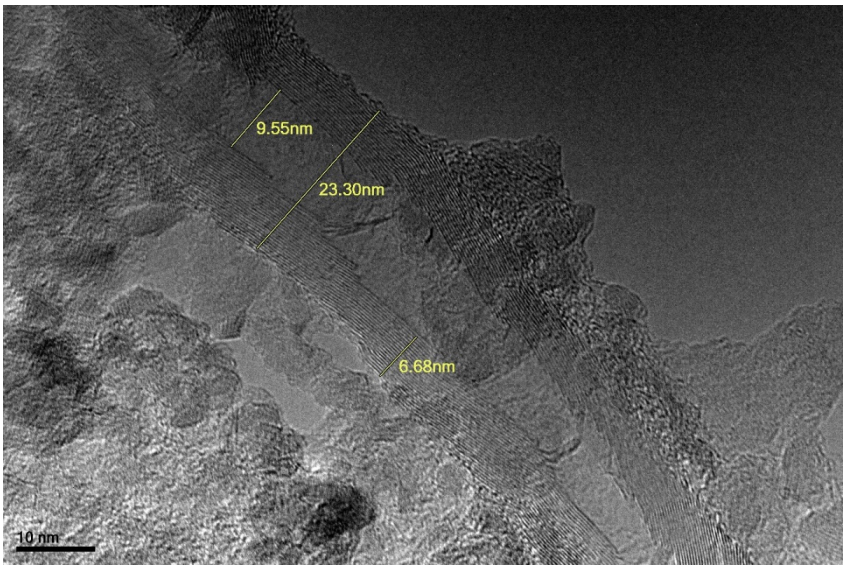

(**a**)

Figure 13. *Cont.*

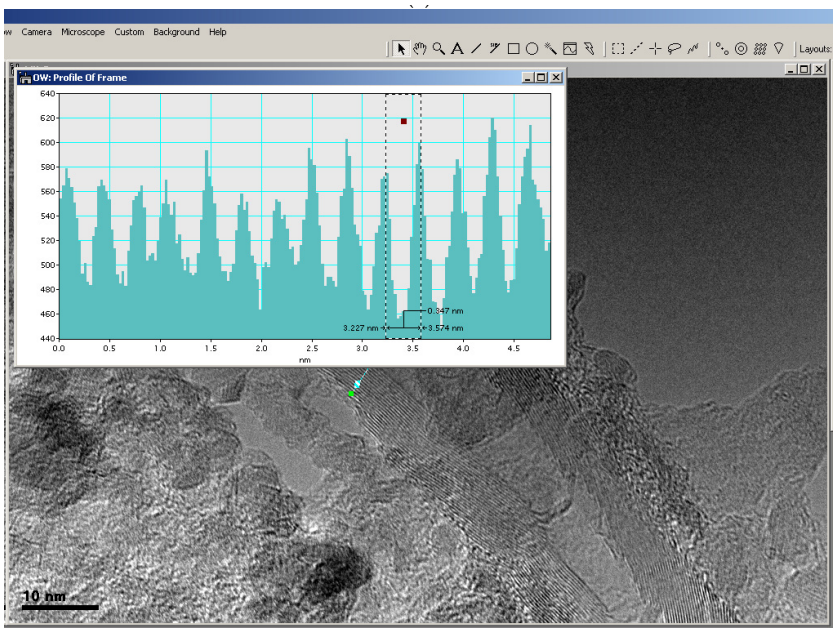

(**b**)

Figure 13. TEM images for spent sample of 5Ni2Mg3SiAl, showing the formation of MWCNT (**a**) and estimated distance between each wall and other within the MWCNT (**b**).

3. Experimental

3.1. Materials

Magnesium acetate tetrahydrate [$Mg(CH_3COO)_2.4H_2O$; Merck, Kenilworth, NJ, USA] and nickel nitrate hexahydrate [$Ni(NO_3)_2{\cdot}6H_2O$; Alfa Aesar, Haverhill, MA, USA] were commercially available. The support of γ-alumina doped with silica (3.0 wt. % $SiO_2/\gamma\text{-}Al_2O_3$) in the shape of pellets was obtained from Inorganic Chemistry Laboratory, Oxford University. Ultrapure deionized water (DI), with a resistivity of 18.2 MΩ.cm, was acquired from a Milli-Q water purification system (Millipore).

3.2. Catalyst Preparation

In the present work, we followed the method of incipient wetness impregnation for the synthesis of DRM catalysts. The required quantities of $Ni(NO_3)_2.6H_2O$ to get 5.0 wt. % loading of nickel oxide, of $Mg(O_2CCH_3)_2.4H_2O$ to get 1.0, 2.0, or 3.0 wt. % loading, and of the support of 3.0 wt. % $SiO_2/\gamma\text{-}Al_2O_3$ were combined and were subsequently crushed. The resultant solid mixture was wetted with DI to form a paste, which was agitated until it was dry. For the homogeneous spreading of the active catalyst and promoter sources over and into the support, the addition of DI and drying steps was repeated. Then, the solid mixture was heated for three hours at 600 °C with a temperature ramping of 3.0 °C/min. The catalysts were denoted, depending on the wt./wt. % loadings of the various components on $\gamma\text{-}Al_2O_3$ support, as follows: 5Ni0Mg3SiAl, 5Ni1Mg3SiAl, 5Ni2Mg3SiAl, and 5Ni3Mg3SiAl.

3.3. Catalyst Activity

DRM experiments, over the prepared catalysts, were performed in a vertically positioned, cylindrical, stainless steel, fixed-bed (0.91 cm i.d. and 300 mm in length) reactor (PID Eng & Tech micro activity reactor, Madrid, Spain), under ambient pressure, in a temperature range of 650 to 850 °C. Catalyst weight of 0.10 g was put over a bed of quartz wool to carry out the activity test. A thermocouple of K-type was fixed at the middle of the bed of the catalyst to monitor the temperature. Before the tests, the catalyst was activated by flowing hydrogen gas (20.0 mL/min) for one hour at 700 °C. The gas mixture was with a volume ratio of 6.0 methane:6.0 carbon dioxide:1.0 nitrogen, and the overall gas rate was 65.0 mL per minute, corresponding to 39,000 mL/h/g_{cat} space velocity. The eluted gases

were directly analyzed by gas chromatography technique (Shimadzu 2014, Kyoto, Japan), equipped with a thermal conductivity detector (TCD). The analysis was repeated at least three times to ensure the reproducibility of the data. The conversion of reactants and the molar ratio of H_2/CO were calculated by the following equations:

$$CH_4 \text{ Conversion } (\%) = \frac{CH_{4\text{ in}} - CH_{4\text{ out}}}{CH_{4\text{ in}}} \times 100 \quad (5)$$

$$CO_2 \text{ Conversion } (\%) = \frac{CO_{2\text{ in}} - CO_{2\text{out}}}{CO_{2\text{ in}}} \times 100 \quad (6)$$

$$H_2/CO = \frac{\text{moles of hydrogen produced}}{\text{moles of CO produced}}. \quad (7)$$

3.4. Catalyst Characterization

N_2 physisorption was employed to evaluate the specific surface area, pore volume, and pore size distribution by using a Micromeritics Tristar II 3020 instrument (Micromeritics, Atlanta, GA, USA), where the Barrett–Joyner–Halenda (BJH) method was used for determining the pore volume and the distribution of pore size.

Powder X-ray diffraction (PXRD) technique was used for recognizing the catalyst structures prior to the reaction by using a Rigaku (Miniflex) diffractometer (Rigaku, Tokyo, Japan). equipped with a Cu K_α X-ray radiation, worked at 40 mA and 40 kV. The scanning of 2θ was within the range of 10–85°, at a step rate of 0.02 degrees. The "X'pert Highscore plus" software helped to assess the data file of the instrument diverse phases, and their scores were checked by using the JCPDS data bank.

TPR measurements were accomplished on a Micromeritics Auto Chem II (Atlanta, GA, USA). A sample amount of seventy mg was placed into the TPR cell and was purged under argon gas for 30 min at 150 °C. Then, the temperature of the sample was decreased to 25 °C. The temperature of the TPR furnace was raised to 1000 °C, at a rate of 10 °C/min, under a continuous flow of 40 mL/min of a mixture of hydrogen and argon gases (1:9 ratio). To monitor the H_2 consumption, a TCD was used.

A Chemisorption Analyzer (Micromeritics Autochem II Atlanta, GA, USA) was used for CO_2 temperature-programmed desorption (CO_2-TPD). A sample of 50.0 mg of catalyst was heated at 400 °C, for one hour, under a flow of 30 mL/min of helium gas, and then, it was cooled down to 50 °C. The flow of CO_2 was retained for one hour, and the sample was washed out by flowing helium gas for the exclusion of any physisorbed CO_2. The temperature was ramped by a ratio of 10 °C/min for recording the catalyst desorption profile. A TCD was used for measuring the CO_2 concentration in the output stream, where the amount of CO_2 during TPD was determined by the integration of the areas under the peaks.

X-ray photoelectron spectroscopy (XPS) was recorded on a JEOL JPS-9200 spectrometer (JEOL, Akishima, Tokyo, Japan) for determining the chemical composition of the catalyst surface by using Mg K_α (hν = 1253.6 eV) under vacuum at 5×10^{-9} Pa, where the C1s peak line at 284.6 eV of the surface adventitious carbon was used as a reference for calibrating the binding energies.

The amount of carbonaceous material, deposited on the surface of the spent catalyst, was evaluated by thermogravimetric analysis (TGA) by using a TGA-15 SHIMADZU analyzer (Shimadzu Corporation, Kyoto, Japan) under aerial atmosphere. A sample of spent catalyst, weighed 10–15 mg, was heated by a rate of 20 °C/min from 25 to 1000 °C for determining the amount of the deposited carbon through weight loss.

The morphology of the catalysts was investigated by using a high-resolution transmission electron microscope (HRTEM model: JEM-2100 F, JEOL, Akishima, Tokyo, Japan), which was run at 200 kV, where the samples were mounted on carbon-coated copper grids for analysis.

4. Conclusions

Four catalysts were prepared with various weight percentage contents of MgO promoter (5Ni0Mg3SiAl, 5Ni1Mg3SiAl, 5Ni2Mg3SiAl, and 5Ni3Mg3SiAl), and these catalysts were tested for DRM to assess the impact of MgO promoter loading. The 2.0 wt. % loading of MgO in 5Ni2Mg3SiAl produced a brilliant promotional effect for the catalytic performance in terms of better conversions and better resistance to the deposition of coke carbon compared to the unpromoted catalyst (5Ni0Mg3SiAl). Improvement was observed for 5Ni2Mg3SiAl catalyst at 800 °C, where the conversions of methane and carbon dioxide were 86% and 91%, respectively. The 5Ni2Mg3SiAl catalyst maintained its activity for 15 h with low carbon deposition (<9.0 wt. %). The investigation of the space velocity stipulated the best GHSV as 39,000 mL/(g_{cat}·h). The enhanced catalytic performance of the promoted catalyst might be ascribed to the promoter-positive modification of the textural properties, its formation of solid solution with nickel oxide, and its increase in metal–support interaction. These findings were verified by the results of the characterization techniques used in this work: N_2 physisorption, H_2-TPR, XRD, XPS, TGA, and TEM.

Author Contributions: A.B., S.O.K. and A.S.A.-F., writing—original draft preparation; R.A. (Rasheed Arasheed), K.A., R.A. (Rawan Ashamari), A.A.I., preparation of catalysts; A.E.A., J.K.A.-D. and A.H.F. contributed to the analysis of the data and proofread the manuscript. All authors have read and agreed to the published version of the manuscript.

Funding: This research was funded by Researchers Supporting Project number (RSP-2021/368), King Saud University, Riyadh, Saudi Arabia.

Acknowledgments: The authors would like to extend their sincere appreciation to Researchers Supporting Project number (RSP-2021/368), King Saud University, Riyadh, Saudi Arabia.

Conflicts of Interest: There are no conflicts to declare.

References

1. Loewert, M.; Serrer, M.-A.; Carambia, T.; Stehle, M.; Zimina, A.; Kalz, K.F.; Lichtenberg, H.; Saraçi, E.; Pfeifer, P.; Grunwaldt, J.-D. Bridging the gap between industry and synchrotron: An operando study at 30 bar over 300 h during Fischer–Tropsch synthesis. *React. Chem. Eng.* **2020**, *5*, 1071–1082. [CrossRef]
2. Ayodele, B.V.; Khan, M.R.; Lam, S.S.; Cheng, C.K. Production of CO-rich hydrogen from methane dry reforming over lanthania-supported cobalt catalyst: Kinetic and mechanistic studies. *Int. J. Hydrogen Energy* **2016**, *41*, 4603–4615. [CrossRef]
3. Saravanan, K.; Ham, H.; Tsubaki, N.; Bae, J.W. Recent progress for direct synthesis of dimethyl ether from syngas on the heterogeneous bifunctional hybrid catalysts. *Appl. Catal. B Environ.* **2017**, *217*, 494–522. [CrossRef]
4. Hanna, J.; Lee, W.Y.; Shi, Y.; Ghoniem, A.F. Fundamentals of electro- and thermochemistry in the anode of solid-oxide fuel cells with hydrocarbon and syngas fuels. *Prog. Energy Combust. Sci.* **2014**, *40*, 74–111. [CrossRef]
5. Al-Fatesh, A.S.; Atia, H.; Ibrahim, A.A.; Fakeeha, A.H.; Singh, S.K.; Labhsetwar, N.K.; Shaikh, H.; Qasim, S.O. CO_2 reforming of CH4: Effect of Gd as promoter for Ni supported over MCM-41 as catalyst. *Renew. Energy* **2019**, *140*, 658–667. [CrossRef]
6. Göransson, K.; Söderlind, U.; He, J.; Zhang, W. Review of syngas production via biomass DFBGs. *Renew. Sustain. Energy Rev.* **2011**, *15*, 482–492. [CrossRef]
7. Usman, M.; Wan Daud, W.M.A.; Abbas, H.F. Dry reforming of methane: Influence of process parameters—A review. *Renew. Sustain. Energy Rev.* **2015**, *45*, 710–744. [CrossRef]
8. Nagaoka, K.; Seshan, K.; Lercher, J.A.; Aika, K.I. Activation mechanism of methane-derived coke (CH_x) by CO_2 during dry reforming of methane—Comparison for Pt/Al_2O_3 and Pt/ZrO_2. *Catal. Lett.* **2000**, *70*, 109–116. [CrossRef]
9. Sepehri, S.; Rezaei, M. Ce promoting effect on the activity and coke formation of Ni catalysts supported on mesoporous nanocrystalline Γ-Al_2O_3 in autothermal reforming of methane. *Int. J. Hydrogen Energy* **2017**, *42*, 11130–11138. [CrossRef]
10. Wu, H.; Wang, L. Shape effect of microstructured CeO_2 with various morphologies on CO catalytic oxidation. *Catal. Commun.* **2011**, *12*, 1374–1379. [CrossRef]
11. Tang, M.; Xu, L.; Fan, M. Effect of Ce on 5 wt% Ni/ZSM-5 catalysts in the CO_2 reforming of CH4 reaction. *Int. J. Hydrogen Energy* **2014**, *39*, 15482–15496. [CrossRef]
12. Navarro, R.M.; Guil-Lopez, R.; Ismail, A.A.; Al-Sayari, S.A.; Fierro, J.L.G. Ni- and PtNi-catalysts supported on Al2O3 for acetone steam reforming: Effect of the modification of support with Ce, la and Mg. *Catal. Today* **2015**, *242*, 60–70. [CrossRef]
13. Kim, T.Y.; Kim, S.M.; Lee, W.S.; Woo, S.I. Effect and behavior of cerium oxide in Ni/γ-Al_2O_3 catalysts on autothermal reforming of methane: $CeAlO_3$ formation and its role on activity. *Int. J. Hydrogen Energy* **2013**, *38*, 6027–6032. [CrossRef]
14. Mattos, L.V.; Rodino, E.; Resasco, D.E.; Passos, F.B.; Noronha, F.B. Partial oxidation and CO_2 reforming of methane on Pt/Al_2O_3, Pt/ZrO_2, and Pt/Ce-ZrO_2 catalysts. *Fuel Process. Technol.* **2003**, *83*, 147–161. [CrossRef]

15. Taherian, Z.; Khataee, A.; Orooji, Y. Nickel-based nanocatalysts promoted over MgO-modified SBA-16 for dry reforming of methane for syngas production: Impact of support and promoters. *J. Energy Inst.* **2021**, *97*, 100–108. [CrossRef]
16. Al-Fatesh, A.S.; Kumar, R.; Fakeeha, A.H.; Kasim, S.O.; Khatri, J.; Ibrahim, A.A.; Arasheed, R.; Alabdulsalam, M.; Lanre, M.S.; Osman, A.I.; et al. Promotional effect of magnesium oxide for a stable nickel-based catalyst in dry reforming of methane. *Sci. Rep.* **2020**, *10*, 13–16. [CrossRef]
17. Karam, L.; Armandi, M.; Casale, S.; El Khoury, V.; Bonelli, B.; Massiani, P.; El Hassan, N. Comprehensive study on the effect of magnesium loading over nickel-ordered mesoporous alumina for dry reforming of methane. *Energy Convers. Manag.* **2020**, *225*, 113470. [CrossRef]
18. Ghods, B.; Meshkani, F.; Rezaei, M. Effects of alkaline earth promoters on the catalytic performance of the nickel catalysts supported on high surface area mesoporous magnesium silicate in dry reforming reaction. *Int. J. Hydrogen Energy* **2016**, *41*, 22913–22921. [CrossRef]
19. Alipour, Z.; Rezaei, M.; Meshkani, F. Effect of alkaline earth promoters (MgO, CaO, and BaO) on the activity and coke formation of Ni catalysts supported on nanocrystalline Al_2O_3 in dry reforming of methane. *J. Ind. Eng. Chem.* **2014**, *20*, 2858–2863. [CrossRef]
20. Shen, J.; Reule, A.A.C.; Semagina, N. Ni/$MgAl_2O_4$ catalyst for low-temperature oxidative dry methane reforming with CO_2. *Int. J. Hydrogen Energy* **2019**, *44*, 4616–4629. [CrossRef]
21. Cho, E.; Lee, Y.H.; Kim, H.; Jang, E.J.; Kwak, J.H.; Lee, K.; Ko, C.H.; Yoon, W.L. Ni catalysts for dry methane reforming prepared by A-site exsolution on mesoporous defect spinel magnesium aluminate. *Appl. Catal. A Gen.* **2020**, *602*, 117694. [CrossRef]
22. Ruckenstein, E. Binary MgO-based solid solution catalysts for methane conversion to syngas. *Catal. Rev-Sci. Eng.* **2002**, *44*, 423–453. [CrossRef]
23. Zhang, R.-J.; Xia, G.-F.; Li, M.-F.; Wu, Y.; Nie, H.; Li, D.-D. Effect of Support on the Performance of Ni-Based Catalyst in Methane Dry Reforming-ScienceDirect. Available online: https://www.sciencedirect.com/science/article/pii/S1872581315300402 (accessed on 5 July 2021).
24. Huang, F.; Wang, R.; Yang, C.; Driss, H.; Chu, W.; Zhang, H. Catalytic performances of Ni/mesoporous SiO_2 catalysts for dry reforming of methane to hydrogen. *J. Energy Chem.* **2016**, *25*, 709–719. [CrossRef]
25. Zhu, J.; Peng, X.; Yao, L.; Shen, J.; Tong, D.; Hu, C. The promoting effect of La, Mg, Co and Zn on the activity and stability of Ni/SiO_2 catalyst for CO_2 reforming of methane. *Int. J. Hydrogen Energy* **2011**, *36*, 7094–7104. [CrossRef]
26. Pompeo, F.; Nichio, N.N.; González, M.G.; Montes, M. Characterization of Ni/SiO_2 and Ni/Li-SiO_2 catalysts for methane dry reforming. *Catal. Today* **2005**, *107–108*, 856–862. [CrossRef]
27. Károlyi, J.; Németh, M.; Evangelisti, C.; Sáfrán, G.; Schay, Z.; Horváth, A.; Somodi, F. Carbon dioxide reforming of methane over Ni–In/SiO_2 catalyst without coke formation. *J. Ind. Eng. Chem.* **2018**, *58*, 189–201. [CrossRef]
28. Kumar Yadav, P.; Das, T.; Mondal, P. Effect of the magnesia and alumina in the modified-supported perovskite-type catalysts for the dry reforming of methane. *Fuel* **2021**, *302*, 121233. [CrossRef]
29. Liu, L.J.; Liu, Y.G.; Gao, X.; Zhang, R.Q.; Zhai, Y.P. Hydrodeoxygenation of bio-oil model compounds over amorphous NiB/SiO2-Al2O3 catalyst in oil-water biphasic system. *Ranliao Huaxue Xuebao/J. Fuel Chem. Technol.* **2017**, *45*, 932–938. [CrossRef]
30. Gobara, H.M. Characterization and catalytic activity of NiO/mesoporous aluminosilicate AlSBA-15 in conversion of some hydrocarbons. *Egypt. J. Pet.* **2012**, *21*, 1–10. [CrossRef]
31. Trasarti, A.F.; Marchi, A.J.; Apesteguía, C.R. Synthesis of menthols from citral on Ni/SiO_2-Al_2O_3 catalysts. *Catal. Commun.* **2013**, *32*, 62–66. [CrossRef]
32. Hu, Y.H.; Ruckenstein, E. The characterization of a highly effective NiO/MgO solid solution catalyst in the CO_2 reforming of CH_4. *Catal. Lett.* **1997**, *43*, 71–77. [CrossRef]
33. Hoste, S.; van de Vondel, D.; van der Kelen, G.P.; de Deken, J. XPS of a steam reforming NiAl2O4 catalyst. *J. Electron Spectros. Relat. Phenom.* **1979**, *16*, 407–413. [CrossRef]
34. Fakeeha, A.H.; Naeem, M.A.; Khan, W.U.; Al-Fatesh, A.S. Syngas production via CO_2 reforming of methane using Co-Sr-Al catalyst. *J. Ind. Eng. Chem.* **2014**, *20*, 549–557. [CrossRef]
35. Rahemi, N.; Haghighi, M.; Babaluo, A.A.; Allahyari, S.; Jafari, M.F. Syngas production from reforming of greenhouse gases CH_4/CO_2 over Ni-Cu/Al2O3 nanocatalyst: Impregnated vs. plasma-treated catalyst. *Energy Convers. Manag.* **2014**, *84*, 50–59. [CrossRef]